FLOW FIELD PREDICTIONS FOR A SLAB DELTA WING AT INCIDENCE

By R. J. Conti, P. D. Thomas, and Y. S. Chou
Lockheed Palo Alto Research Laboratory

SUMMARY

Theoretical results are presented for the structure of the hypersonic flow field of a blunt slab delta wing at moderately high angle of attack. Special attention is devoted to the interaction between the boundary layer and the inviscid entropy layer. The results are compared with experimental data.

The three-dimensional inviscid flow is computed numerically by a "marching" finite-difference method. Attention is concentrated on the windward side of the delta wing, where detailed comparisons are made with the data for shock shape and surface pressure distributions. Surface streamlines are generated, and used in the boundary layer analysis.

The three-dimensional laminar boundary layer is computed numerically using a specially-developed technique based on small cross-flow in streamline coordinates. In the rear sections of the wing the boundary layer decreases drastically in the spanwise direction, so that it is still submerged in the entropy layer at the centerline, but surpasses it near the leading edge. Predicted heat transfer distributions are compared with experimental data.

This work was sponsored by the Lockheed Independent Research Program as part of the analysis of Space Shuttle flow fields.

INTRODUCTION

The main objective of this study was to test a complete three-dimensional flow field prediction, including inviscid flow and boundary layer, by comparison with detailed wind-tunnel measurements. During the development of the computational tools for three-dimensional flow, the computer codes were checked by calculating flow over simple shapes (such as sharp and blunted cones) for which the flow field is well known. The present effort takes a step beyond that by dealing with a more complicated shape. The slab delta wing was chosen for two reasons: good experimental results are available in the work of Whitehead and Dunavant (Ref. 1), and this shape, which is of interest to Space Shuttle applications, poses a more severe test than, say, a typical shuttle fuselage. This is so because the slab delta wing sustains a combination of inboard and outboard transverse pressure gradients, due to the fact that the peak pressure is located at the centerline near the nose, and near the leading edge in downstream sections. As a consequence, both the inviscid and viscous analyses are tested under a combination of effects. The next step, reserved for future work, is to calculate the flow field for a complete shuttle configuration, including fuselage and wings.

There were two secondary objectives in this study. The first was to pursue a complete calculation to its final stage, that is, to an estimate of heat transfer, in order to gain an appreciation for the difficulties involved and of the accuracy needed at the different stages of computation of inviscid and boundary-layer flows. In this respect it was somewhat surprising to find that the calculation of three-dimensional boundary layer demands considerable accuracy in the inviscid calculations. The suspicion that finite-difference calculation of the inviscid flow might constitute "accuracy overkill" did not materialize in this study.

The other secondary objective was to assess the interference of boundary layer and inviscid entropy layer. Unfortunately, it turned out that the model was not long enough to produce an extreme case of interference, but nevertheless the boundary layer did become larger than the

entropy layer in the downstream sections near the leading edge. In this case the conventional first-order boundary layer calculation yielded acceptable values of heat transfer, and, when corrected grossly for edge conditions, the change in heat transfer was small. Nevertheless, this evidence is not sufficient to conclude that the interference between boundary layer and entropy layer is negligible.

MODEL AND STREAM CONDITIONS

(Figure 1)

The inviscid flow was calculated with the method of Thomas, et al. described in Ref. 2. This is a marching finite-difference method for supersonic three-dimensional flows. Some of the main features are a sharp-shock treatment for the bow shock, nonlinear stretching of coordinates in the radial and meridional directions (about the longitudinal axis) to resolve steep gradients in the flow, acceptance of a wide range of body geometries, and perfect-gas or equilibrium-air options. The subsonic and transonic parts of the flow near the nose were calculated, in this case, with the method of Inouye, Rakich and Lomax (Ref. 3). The stream conditions and body shape corresponded exactly to those of the wind-tunnel experiments (Ref. 1). Since real-gas effects were negligible in the experiments, the flow was calculated using the perfect-gas option.

The body was a flat, slab delta wing with spherically-blunted nose and cylindrical leading edges, having a sweep angle of 80 degrees. The angle of attack was 20 degrees. The Mach number was 9.6, ratio of specific heats 1.4, Reynolds number based on thickness 10^5, stagnation pressure 45 atm, and stagnation temperature 920 degrees Kelvin. The wall-temperature ratio was 0.32.

SKETCH OF MODELS. (ALL DIMENSIONS ARE IN CM)

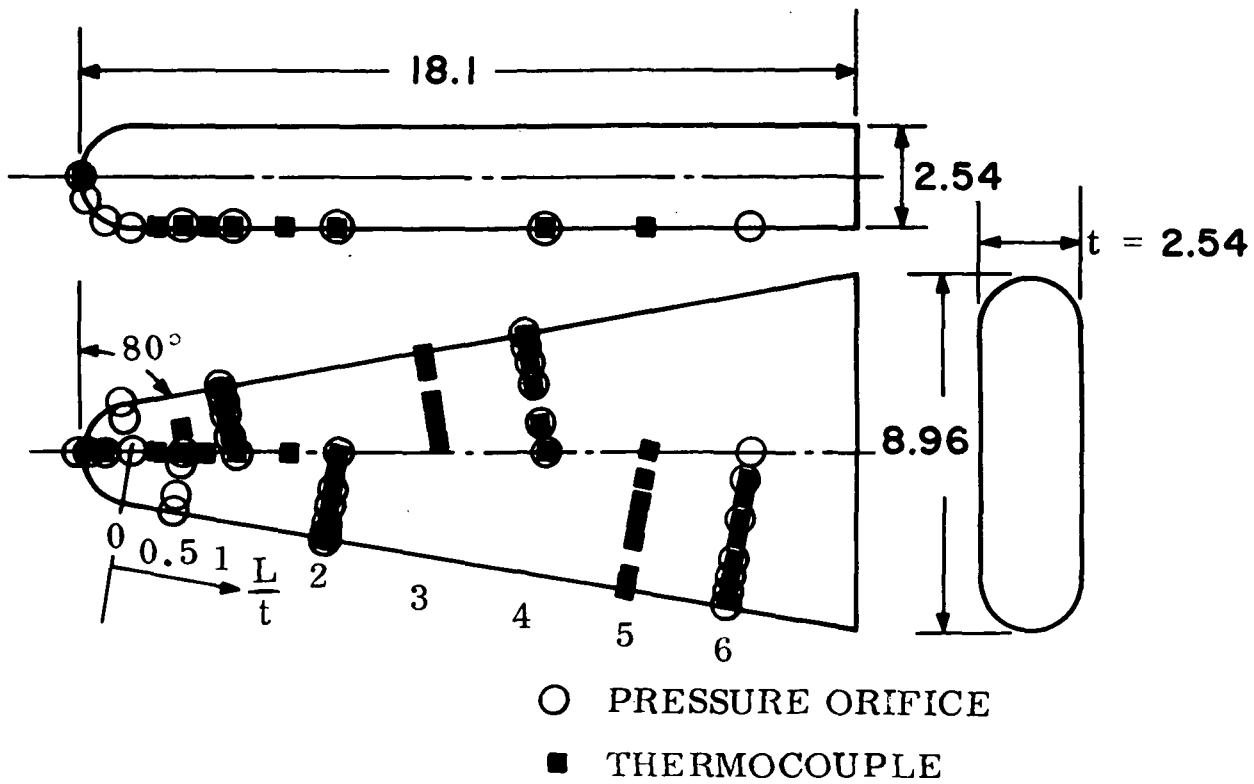

Figure 1

SHOCK SHAPE AND SURFACE STREAMLINE PATTERN
(Figure 2)

The flow field was calculated over the entire cross section (windward and leeward sides) in the forward third of the body. When the cross flow became supersonic the calculation was cut off at the geometric leading edge, and attention was focused on the windward part of the wing. At this angle of attack it is expected that viscous effects in the leeward side are such that the inviscid calculation is irrelevant.

The calculated shock shape agrees well with the measured one, but this is not considered to be a stringent test because shock shape is an insensitive characteristic. The data points were taken from a small photograph, and slight discrepancies with the calculated shock are probably due to reading errors and are unimportant.

The surface streamlines were obtained with a separate calculation, by integrating the inviscid surface velocity. Knowledge of the velocity vector and the unit vector normal to the surface is sufficient to calculate the curvature vector, its projections along and normal to streamlines, and the metric of a streamline-oriented curvilinear coordinate system. In addition, the streamline routine calculates inputs for the boundary layer, such as the transformed longitudinal coordinate (which includes compressibility and edge-property effects) and edge velocity gradient.

The figure shows the effects of transverse pressure gradients on streamline shape. Near the nose, where the peak pressure is at the centerline, all streamlines curve toward the leeward side. Downstream, where there is a pressure ridge near the leading edge, some streamlines are turned leeward and some are turned toward the centerline.

SHOCK SHAPE AND SURFACE STREAMLINE PATTERN
80° SLAB DELTA WING, α = 20°, M_∞ = 9.6, γ = 1.4

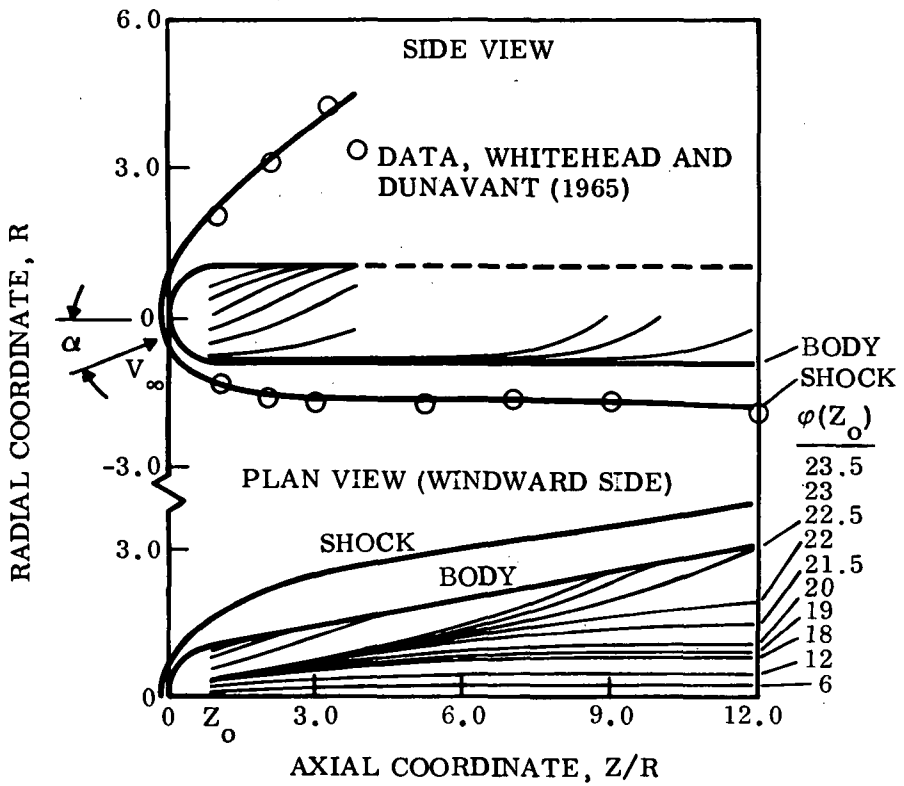

Figure 2

WINDWARD CENTERLINE PRESSURE

(Figure 3)

The surface pressure on the centerline is plotted versus the axial coordinate. The figure shows the rapid expansion around the nose, followed by a slight overexpansion (typical of blunt-nosed bodies) and a subsequent recompression. The agreement between theory and experiment is excellent. The theoretical curve shows a slight oscillation at the juncture between the spherical nose and the flat underside of the wing. This oscillation is induced in the numerical results by the discontinuity in curvature at the juncture.

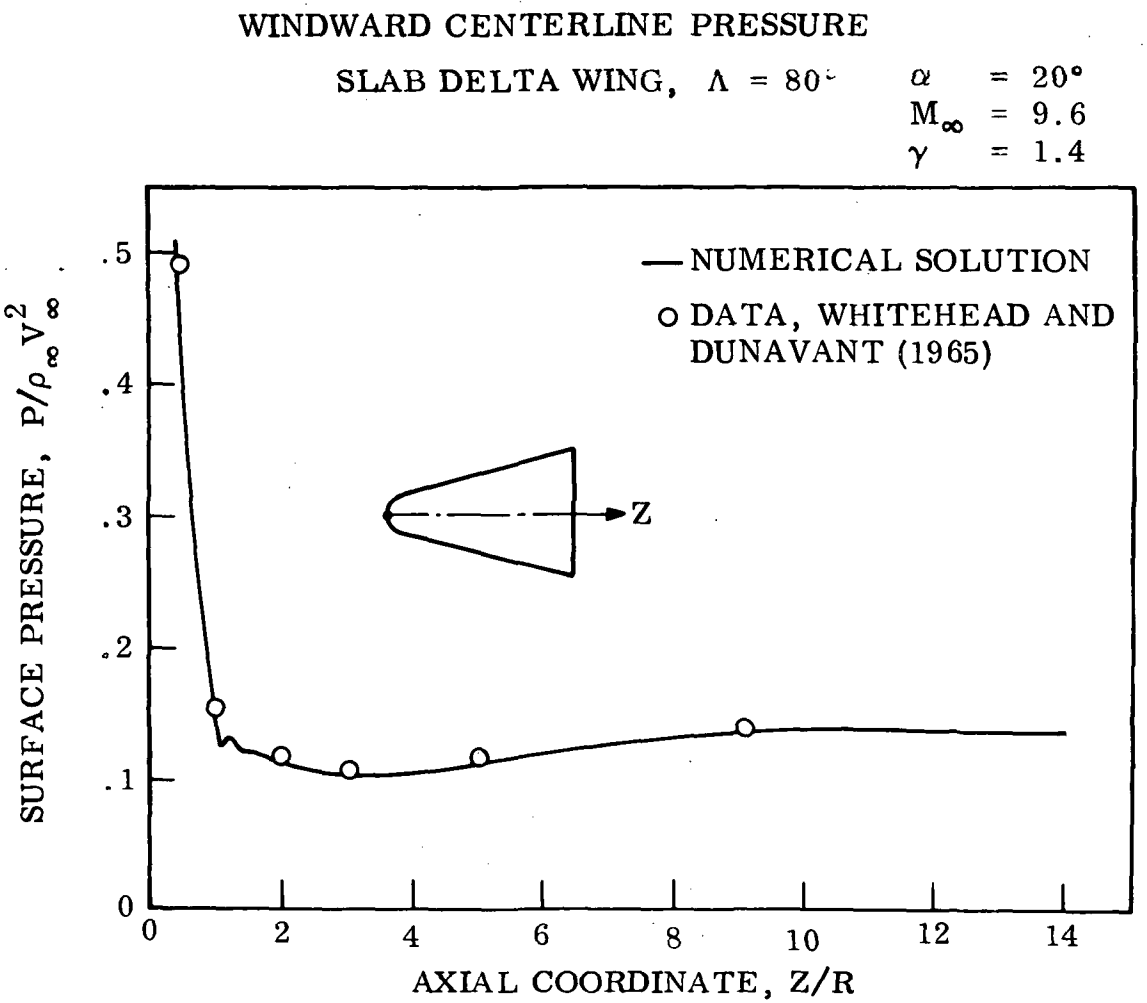
WINDWARD CENTERLINE PRESSURE
SLAB DELTA WING, Λ = 80°
α = 20°
M∞ = 9.6
γ = 1.4
— NUMERICAL SOLUTION
o DATA, WHITEHEAD AND DUNAVANT (1965)
Z
SURFACE PRESSURE, P/ρ∞V∞²
.5
.4
.3
.2
.1
0
0
2
4
6
8
10
12
14
AXIAL COORDINATE, Z/R

Figure 3

SURFACE PRESSURE DISTRIBUTIONS IN PLANES NORMAL TO THE LEADING EDGE

(Figure 4)

Surface pressure distributions are plotted versus distance along the surface, measured from the geometric leading edge, for several downstream locations. Notice that the downstream distance L is measured parallel to the leading edge, rather than to the centerline. Similarly, the surface location S is normal to the leading edge, not the centerline. This change in coordinates was needed to accommodate the experimental data. It has a slight effect on the shape of the curves, notably near the nose where the pressure maximum appears to be off-centerline and the curve appears to be nonsymmetric about the centerline. The agreement between theory and experiment is good, except at isolated points where discrepancies remain unexplained.

SURFACE PRESSURE DISTRIBUTIONS IN PLANES NORMAL TO THE LEADING EDGE
SLAB DELTA WING, $\Lambda = 80^{o}$, $\gamma = 1.4$, $\alpha = 20^{o}$, $M_{\infty} = 9.6$

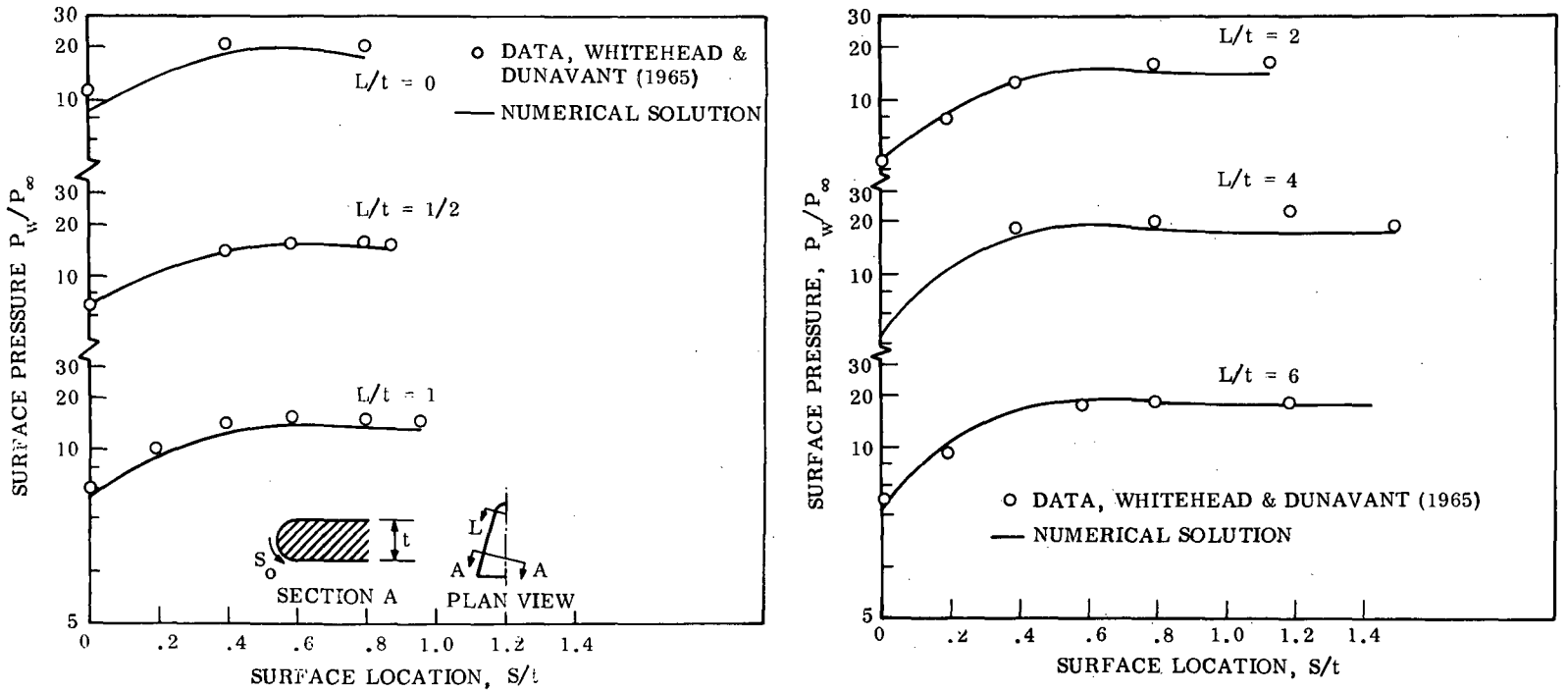

Figure 4

ENTHALPY PROFILE
(Figure 5)

The distribution of enthalpy across the shock layer at about 13 nose radii from the nose is shown for two locations: the centerline and a point near the leading edge. The entropy layer, a region of hot, slow-flowing gas that traversed the bow shock near the nose (where the shock is strongest) is located near the surface. It can be seen that the entropy layer is much thicker at the centerline (about 0.30 nose radii) than near the leading edge (about 0.05 nose radii). This is a feature unknown to axisymmetric flows, where the entropy layer thins out uniformly in the downstream direction.

The presence of the entropy layer extracts a heavy tax from the computational scheme since, in order to resolve the steep gradients in the layer and maintain computational stability, it is necessary to concentrate mesh points near the surface. In the present computational scheme this is done by "stretching" the normal coordinate. Moreover, we have found that a preset stretching (either constant or variable in the downstream direction) is not sufficient to solve the difficulty. We have had to resort to a self-adjusting scheme that will regulate the concentration of mesh points during execution of the calculation. It is emphasized that the difficulty is not just one of losing detail in the entropy layer (which would be affected by viscous effects in any case) but one of losing the integrity of the whole calculation unless every region of the flow is properly resolved. The need to change the stretching factor in the meridional direction is not as critical, in particular in the present scheme where the mesh size is proportional to the shock layer thickness, and therefore the mesh is automatically refined at places (such as leading edges) where the shock layer is thinner.

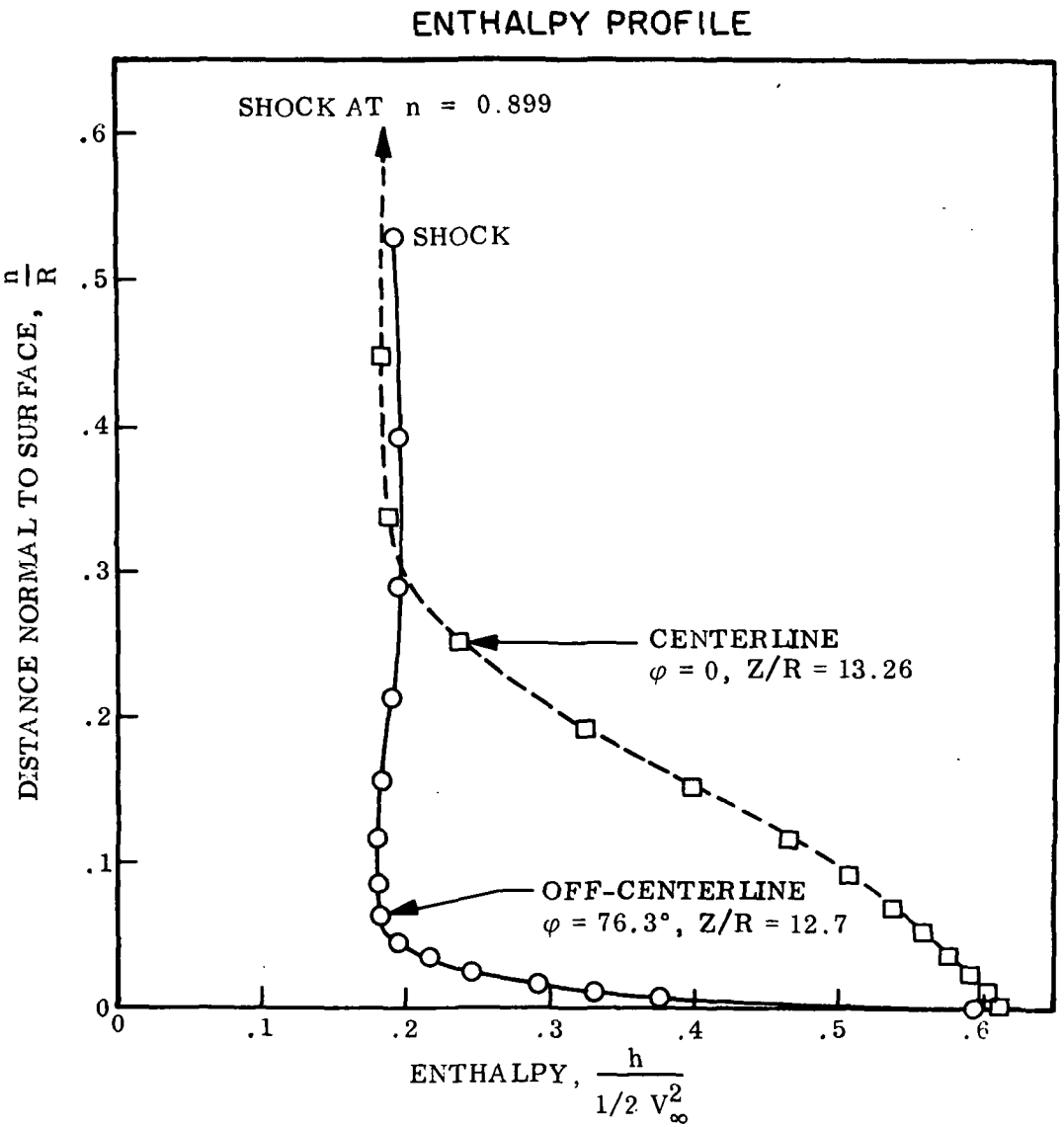
ENTHALPY PROFILE
SHOCK AT n = 0.899
SHOCK
CENTERLINE
φ = 0, Z/R = 13.26
OFF-CENTERLINE
φ = 76.3°, Z/R = 12.7
DISTANCE NORMAL TO SURFACE, n/R
ENTHALPY, h/(1/2 V∞²)
0
.1
.2
.3
.4
.5
.6

Figure 5

BOUNDARY-LAYER CALCULATIONS

Heat Transfer Distribution Along Centerline

(Figure 6)

The three-dimensional laminar boundary layer was calculated with a technique developed by Y. S. Chou for this particular application. The technique is based on small cross flow in streamline coordinates. This places no restriction on the curvature of inviscid streamlines, but assumes that inside the boundary layer the deviation from inviscid streamlines is small, which is a good assumption for hypersonic flow over cold walls. For the sake of simplicity it is assumed that the Prandtl number is constant (not necessarily unity), the product of density and viscosity does not vary across the layer (it is evaluated at the "reference conditions") and the density is inversely proportional to the enthalpy. The theory does not resort to "local flat plate" or self-similarity assumptions. The method has been tested successfully on ellipsoids and blunted cones at incidence.

The centerline distribution of heat transfer coefficient, referred to the stagnation-point value, is shown versus the axial coordinate in nose radii. The striking feature about this distribution is its serpentine character, most of which can be attributed to cross flow effects. This is somewhat surprising in view of the simple geometry of the delta wing but, as stated previously, the cross flow varies and changes sign as one moves downstream. The character of the theoretical curve seems to be supported by the experimental results. The general agreement between theory and experiment is good by heat-transfer standards, the largest discrepancy being about 25 percent. The solid square at the end of the curve indicates the effect of making an entropy-layer correction, to be discussed later.

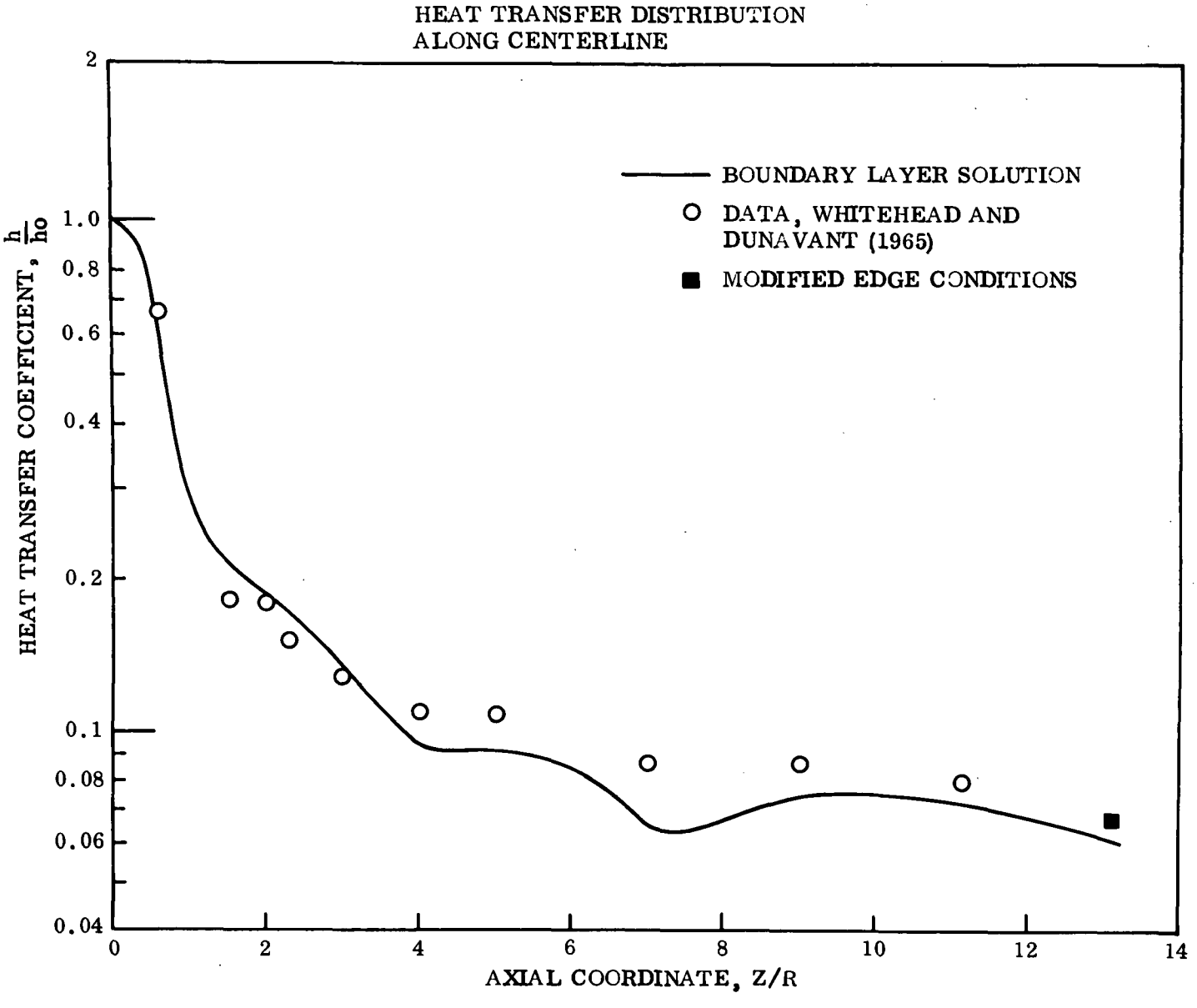
HEAT TRANSFER DISTRIBUTION
ALONG CENTERLINE
BOUNDARY LAYER SOLUTION
DATA, WHITEHEAD AND
DUNAVANT (1965)
MODIFIED EDGE CONDITIONS
HEAT TRANSFER COEFFICIENT, h/ho
AXIAL COORDINATE, Z/R
2
1.0
0.8
0.6
0.4
0.2
0.1
0.08
0.06
0.04
0
2
4
6
8
10
12
14

Figure 6

SPANWISE DISTRIBUTION OF BOUNDARY-LAYER THICKNESS

(Figure 7)

The boundary layer varies drastically in the spanwise direction due to three-dimensional effects. At about 12 nose radii from the nose (L/t = 6) the physical thickness varies by about a factor of three from the centerline (where it is thicker) to the leading edge. This decrease in thickness towards the leading edge corresponds to an approximately equal increase in heat transfer, in spite of the fact that the pressure is lower at the leading edge. It will be recalled that the entropy layer decreases by a factor of five in the same spanwise region, and therefore the boundary layer thickens with respect to the entropy layer in the outboard direction.

SPANWISE DISTRIBUTION OF BOUNDARY-LAYER THICKNESS AT L/t = 6

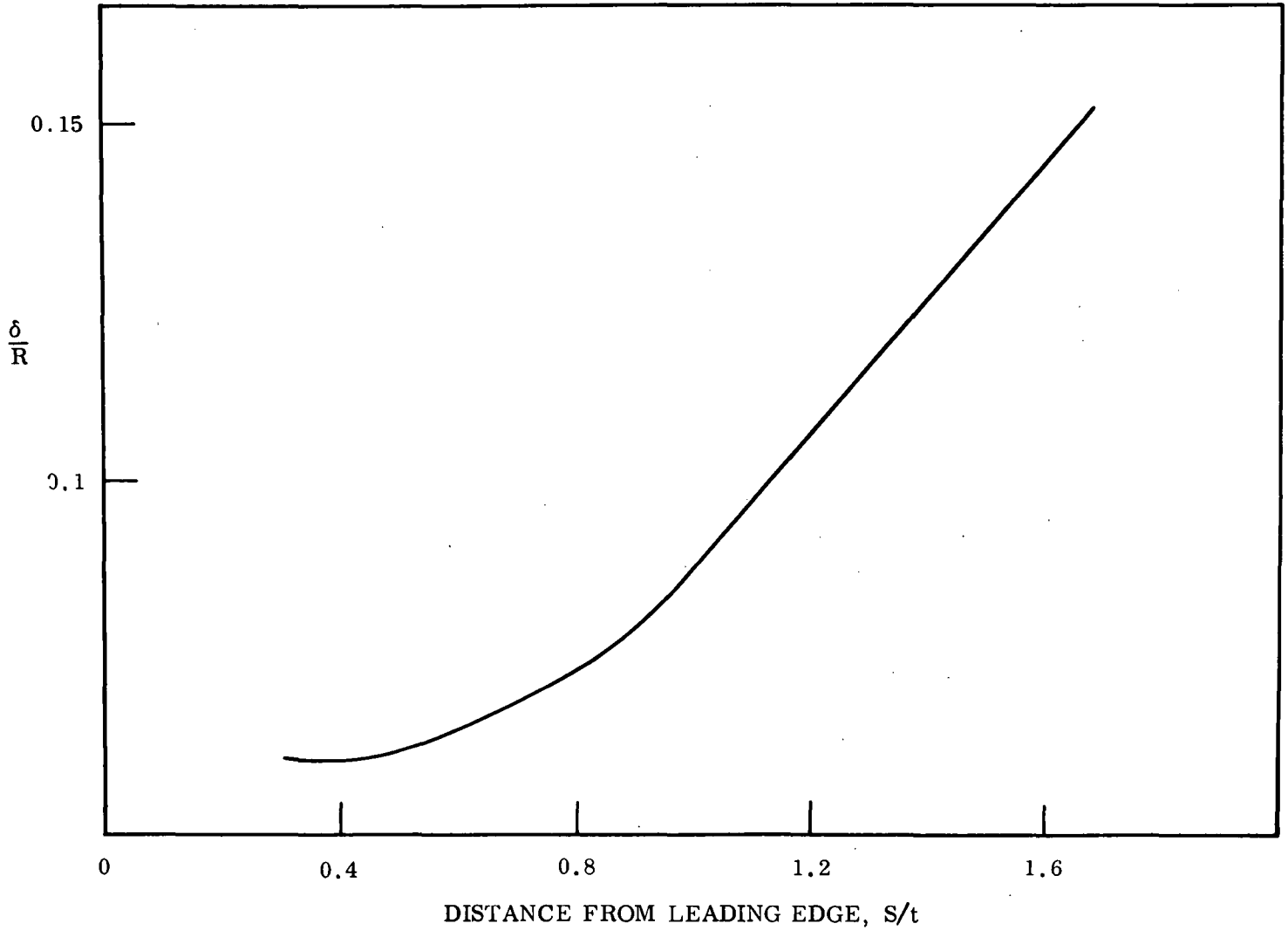

Figure 7

SPANWISE HEAT TRANSFER DISTRIBUTION

(Figure 8)

The absolute heat transfer, represented by the Stanton number, is plotted versus distance from the leading edge at two downstream locations: $L/t = 3$ (about 6 nose radii) and $L/t = 6$ (about 12 nose radii). As indicated previously, the boundary layer thins out in the outboard direction, and the heat transfer follows suit. The general agreement between theory and experiment is good, the largest discrepancy being about 25 percent. This occurs at $L/t = 6$, at one inboard and one outboard point, and remains unexplained. The correction for entropy layer is small, about 10 percent in all cases. It always increases the heat transfer, which seems to be in the direction of the experimental data for the inboard point, but opposite to it for the outboard point.

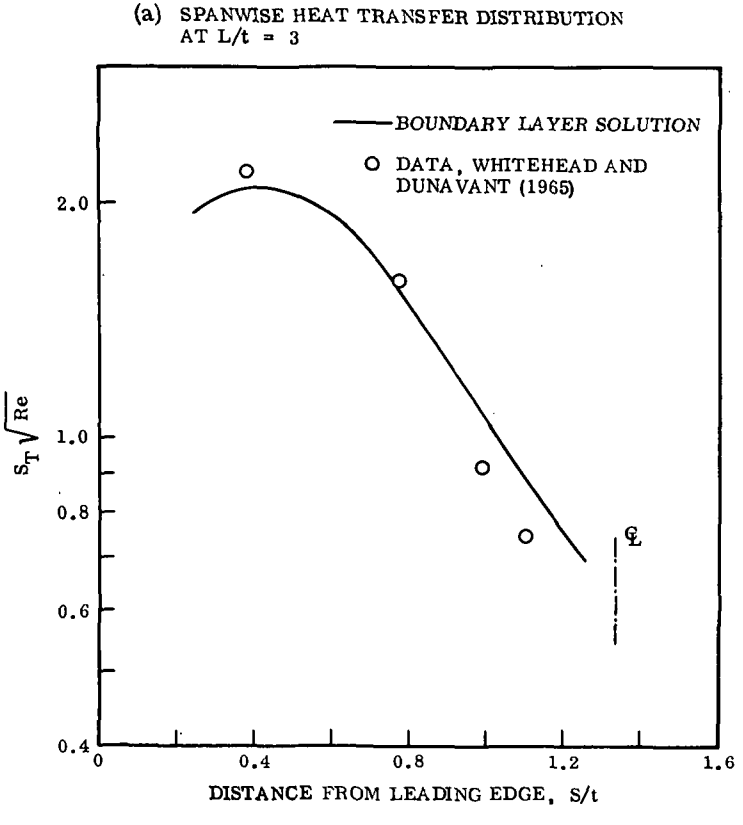
(a) SPANWISE HEAT TRANSFER DISTRIBUTION
AT L/t = 3
BOUNDARY LAYER SOLUTION
DATA, WHITEHEAD AND
DUNAVANT (1965)
$S_T\sqrt{Re}$
2.0
1.0
0.8
0.6
0.4
0
0.4
0.8
1.2
1.6
DISTANCE FROM LEADING EDGE, S/t
℄

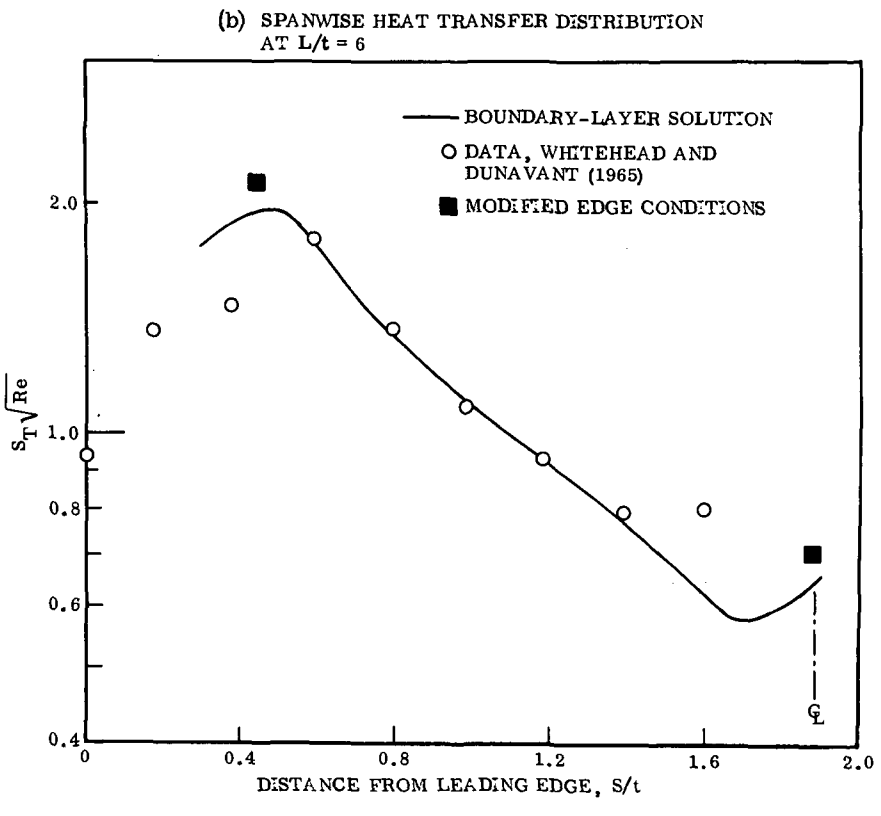
(b) SPANWISE HEAT TRANSFER DISTRIBUTION
AT L/t = 6
BOUNDARY-LAYER SOLUTION
DATA, WHITEHEAD AND
DUNAVANT (1965)
MODIFIED EDGE CONDITIONS
$S_T\sqrt{Re}$
2.0
1.0
0.8
0.6
0.4
0
0.4
0.8
1.2
1.6
2.0
DISTANCE FROM LEADING EDGE, S/t
℄

Figure 8

ENTHALPY PROFILE IN THE BOUNDARY LAYER

(Figure 9)

It will be recalled that near the base of the model, at about 13 nose radii from the nose, both boundary layer and entropy layer thin out in the outboard direction, the boundary layer by a factor of three, the entropy layer by a factor of five (see figures 5 and 7). The boundary layer, which is about half the thickness of the entropy layer at the centerline, thus becomes somewhat thicker than the entropy layer near the leading edge. In an attempt to estimate the magnitude of the interaction we calculated the boundary layer twice: once in the classical manner, where edge conditions match the inviscid flow at the wall, and once by patching the edge conditions to those in the interior of the inviscid flow, at the point where the physical "edge" of the boundary layer would be. Partial results are shown in figure 9 in the form of enthalpy profiles in the inviscid flow, in the classical boundary layer, and with modified edge conditions.

It can be seen that the enthalpy profile changes substantially, both in magnitude and character. The classical boundary layer has a monotonic profile, the modified one a bulging profile. This is particularly marked at the leading-edge location, where the edge is hotter than the wall in the classical case and colder than the wall in the modified version. Nevertheless, the heat transfer changes by less than 10 percent, as was indicated previously (see figures 6 and 8b). This partial evidence tends to indicate that heat transfer is not very sensitive to entropy layer interaction, but more work is needed before a general conclusion can be reached.

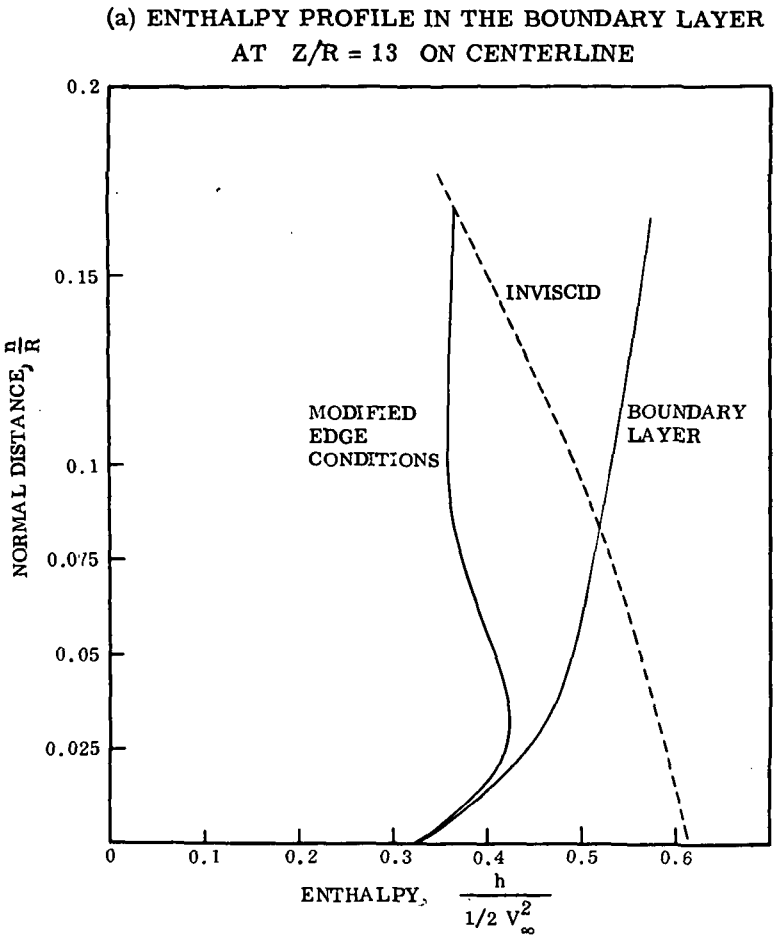
(a) ENTHALPY PROFILE IN THE BOUNDARY LAYER
AT Z/R = 13 ON CENTERLINE
NORMAL DISTANCE, n/R
0.2
0.15
0.1
0.075
0.05
0.025
INVISCID
MODIFIED
EDGE
CONDITIONS
BOUNDARY
LAYER
0
0.1
0.2
0.3
0.4
0.5
0.6
ENTHALPY, h / 1/2 V∞²

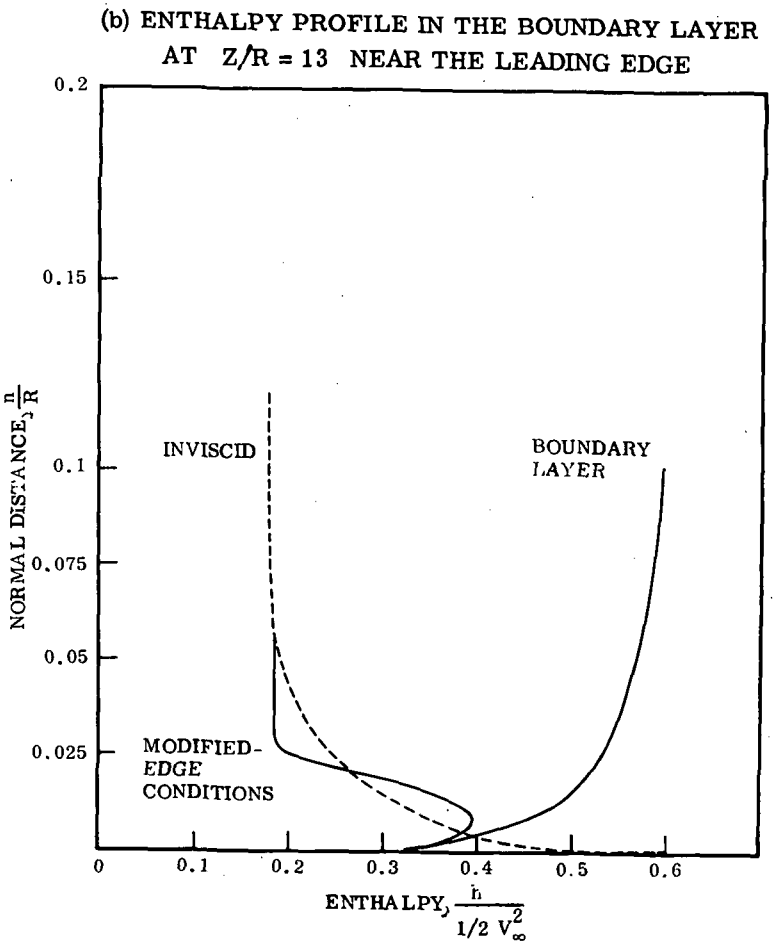
(b) ENTHALPY PROFILE IN THE BOUNDARY LAYER
AT Z/R = 13 NEAR THE LEADING EDGE
NORMAL DISTANCE, n/R
0.2
0.15
0.1
0.075
0.05
0.025
INVISCID
BOUNDARY
LAYER
MODIFIED-
EDGE
CONDITIONS
0
0.1
0.2
0.3
0.4
0.5
0.6
ENTHALPY, h / 1/2 V∞²

Figure 9

REFERENCES

1. Whitehead, A. H. and Dunavant, J. C.: "A Study of Pressure and Heat Transfer over an 80° Swept Slab Delta Wing in Hypersonic Flow." NASA TND-2708, 1965.
2. Thomas, P. D.; Vinokur, M.; Bastianon, R.; and Conti, R.: "Numerical Solution for the Three-Dimensional Hypersonic Flow Field of a Blunt Delta Body." AIAA Paper 71-596, 1971.
3. Inouye, M; Rakich, J. V.; and Lomax, H.: "A Description of Numerical Methods and Computer Programs for Two-Dimensional and Axisymmetric Supersonic Flow over Blunt-Nosed and Flared Bodies." NASA TND-2970, 1965.